Proceeding Paper

Dynamic Analysis of Water Surface Extent and Climate Change Parameters in Zarivar Lake, Iran [†]

Ehsan Rostami [1], Rasool Vahid [2], Arastou Zarei [1,*] and Meisam Amani [3]

1 School of Surveying and Geospatial Engineering, College of Engineering, University of Tehran, Tehran 1439957131, Iran; ehsan.rostami@ut.ac.ir
2 Environmental Dynamics Program, University of Arkansas, Fayetteville, AR 72701, USA; rvahidbe@uark.edu
3 WSP Environment and Infrastructure Canada Limited, Ottawa, ON K2E 7L5, Canada; meisam.amani@wsp.com
* Correspondence: arastou.zarei@ut.ac.ir
† Presented at the 5th International Electronic Conference on Remote Sensing, 7–21 November 2023; Available online: https://ecrs2023.sciforum.net/.

Abstract: Wetlands are valuable natural resources that provide many services to both the environment and humans. Over the past several decades, climatic change and human activities have had a considerable impact on the water level of wetlands. Zarivar Lake, located in the northwestern region of Iran, represents a significant ecological unit and aquatic ecosystem. In this study, from 2015 to 2022, the relationship between seasonal changes in Zarivar Lake's waterbody (LWB) area and weather factors like precipitation, evapotranspiration, and the temperature of the lake's surface water (LSWT) were examined. For this purpose, the Google Earth Engine (GEE) cloud platform, a powerful and fast tool for processing the time series of images, was used. The LWB was extracted by utilizing the average images of the dual-polarized SAR Sentinel-1 imagery for each season. Furthermore, meteorological parameters encompass the utilization of the Landsat-8 satellite's thermal band to determine LSWT by using statistical mono-window (SMW), the CHIRPS rainfall model data for assessing precipitation levels, and the employment of MODIS evapotranspiration products in the form of 8-day data. The study revealed significant correlations between variations in Zarivar Lake's waterbody area and meteorological factors. Correlation coefficients indicated a positive relationship between LWB area and precipitation during the winter ($r = 0.67$) and spring ($r = 0.73$), while weaker positive correlations were observed in the summer ($r = 0.29$) and fall ($r = 0.30$). Conversely, the LWB area showed a relative relationship with LSWT, with positive correlations in winter ($r = 0.10$) and spring ($r = 0.26$), and negative correlations in summer ($r = -0.30$) and fall ($r = -0.07$). Additionally, evapotranspiration parameters aligned with precipitation changes throughout the seasons, highlighting the significant influence of climate on Zarivar Lake.

Keywords: Remote Sensing; Zarivar Lake; water surface extent; Google Earth Engine (GEE)

1. Introduction

Lakes are among the most important water resources for human consumption, agricultural development, and industrial production. They are also recognized as an integral part of the surface water cycle [1]. Changes in the area of lakes are significant indicators of climate and environmental changes at regional and global levels [2,3]. It is predicted that climate change, along with urbanization, population growth, and high-water consumption, will intensify pressure on natural resources [4–6]. The main reasons for the reduction and destruction of water in lakes include changes in land use, agricultural development, diversion of river water through dam construction, sewage infrastructure, water and air pollution, and discharge of waste materials into lakes [7–9]. Therefore, precise monitoring of water body changes in lakes is of great importance for water resource management [10].

Despite traditional field measurements, remote sensing images have high coverage, low cost, and the ability to acquire real-time information. Therefore, remote sensing science has a wide range of applications in monitoring lake water bodies (LWB) at regional and global scales [11]. There are various methods for extracting LWB from multi-spectral and radar images. Some of the commonly used methods include band combination techniques in images, classification-based methods, and threshold-based techniques. Synthetic aperture radar (SAR) technology is a highly suitable option for monitoring surface waters and wetlands on a seasonal and annual basis [12,13]. SAR has numerous features that make it an ideal tool for monitoring water bodies over time. SAR has the capability of imaging day and night, and it can penetrate through clouds in near real time. These are often limitations for optical and infrared satellite sensors [14].

Hydro-climatic factors play a fundamental role in determining water volume, area, and predictable criteria. For example, Lake Mead, formed above the Hoover Dam and alongside the Colorado River in the southwestern United States, demonstrates that net evaporation and precipitation changes are related to the water volume of the lake [15]. From this perspective, identifying the effects of climate factors on changes in the water area of lakes is of great importance. In a study by Al-Barqouni et al. [8], the correlation between the Land-Water Boundary (LWB) area of Burdur, Egirdir, and Beysehir lakes and the parameter of lake surface water temperature (LSWT) was investigated. Time series images from Landsat-5 and Landsat-8 were utilized for this research. The findings indicated that as the water surface temperature of the lakes increased over time, the water area decreased. The correlation coefficients between LWB area and LSWT in Burdur, Beysehir, and Egirdir lakes were reported as -0.20, -0.41, and -0.76, respectively. In another study, Lichen Lu et al. [16] investigated nine lakes of the Yungui Plateau in Yunnan province, China. In this research, using Landsat satellite images from 1988 to 2021 and with water indices. The findings showed that the relationship between the LWB area and the rainfall data of the CHIRPS model has a direct relationship (positive correlation) and an opposite relationship (negative correlation) with the temperature and evaporation data. Also, the results showed that the evaporation factor was more effective in shallow lakes than in deep lakes.

The contributions of the present study are as follows: (1) to initially detect and analyze the spatiotemporal variations in water surface areas and LSWT of Zarivar Lake; and (2) to investigate the seasonal changes in the water surface extent of Zarivar Lake from 2015 to 2022 and examine their connections with meteorological indicators, including precipitation and evapotranspiration.

2. Materials

2.1. Study Area

Zarivar Lake is located in Kurdistan province in the northwest of Iran (Figure 1). This lake is the largest freshwater lake in the province and is one of the most valuable ecosystems in Kurdistan province and western Iran, which has created suitable living conditions for plants and animals. So far, 29 species of plants, 74 species of birds, 9 species of fish, 2 species of mammals, 3 species of amphibians, and 2 species of reptiles have been identified in the ecosystem of this region [17]. Zarivar Lake is located between a longitude of $46°6'$ to $46°10'$ and a latitude of $35°30'$ to $35°35'$ and is located 3 km away from Marivan city and its mean height is 1275 m above sea level. Its minimum depth is 6 m and its maximum depth is 12 m.
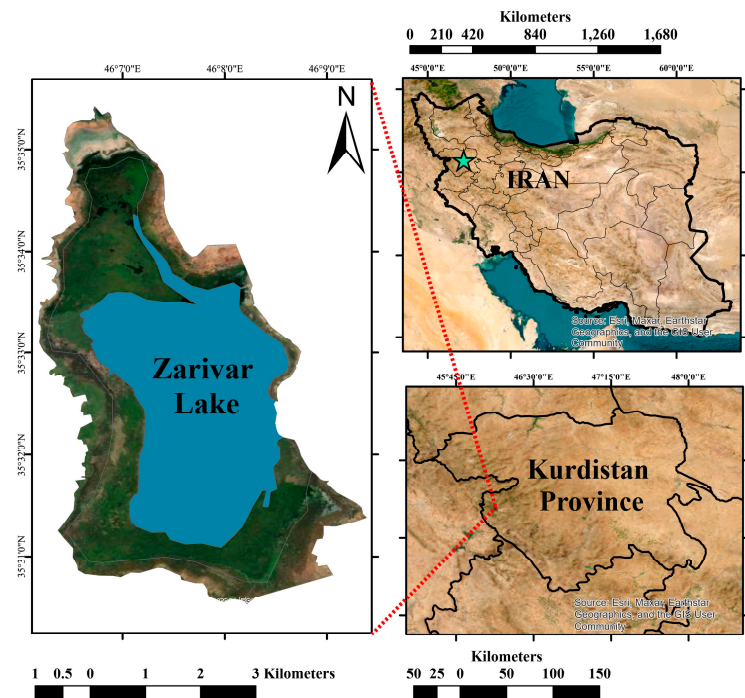
Figure 1. Location of Zarivar Lake in the district of Kurdistan province.

2.2. Earth Observation Data

In the context of earth observation and meteorological datasets for our research, a multifaceted approach to gathering crucial environmental data is employed. To gauge the precipitation dynamics, we relied on daily rainfall data from the CHIRPS model, allowing us to compute the average rainfall within our study area for each season [18,19]. Complementing this, we turned to the MOD16A2.006 evapotranspiration product, which affords users the ability to access 8-day satellite imagery at an impressive 500 m resolution. Leveraging this resource, the evapotranspiration rates are extracted, averaging them across the different seasons [20].

Additionally, we incorporated Sentinel-1 SAR data into our toolkit. This invaluable resource facilitated the precise extraction of water surface area information, enhancing our capacity to comprehensively analyze the study area's hydrological dynamics [21]. Also, the thermal band in the Landsat-8 satellite images measures the radiance emitted by the Earth's surface, allowing for the calculation of water temperature. These data are crucial for understanding changes in aquatic ecosystems, tracking climate-driven variations, and assessing the health of lakes and other water bodies [22].

3. Methodology

According to Figure 2, the implementation flowchart includes four parts: (I) firstly, for Sentinel-1 satellite images, the images as average composites in each season have been collected; (II) secondly, using Landsat-8 satellite images of surface reflectance products, the lake water surface temperature with the SMW algorithm have been estimated. (III) At this step, the products of daily rainfall data from the CHIRPS model were used to calculate the average amount of rainfall in the study area in each season. Also, for the evapotranspiration product MOD16A2.006, which provides users with 8 days with a resolution of 500 m, the amount of evapotranspiration was obtained as an average in each season. (IV) In the fourth step, the relationship between changes in water area over time and meteorological data were investigated.
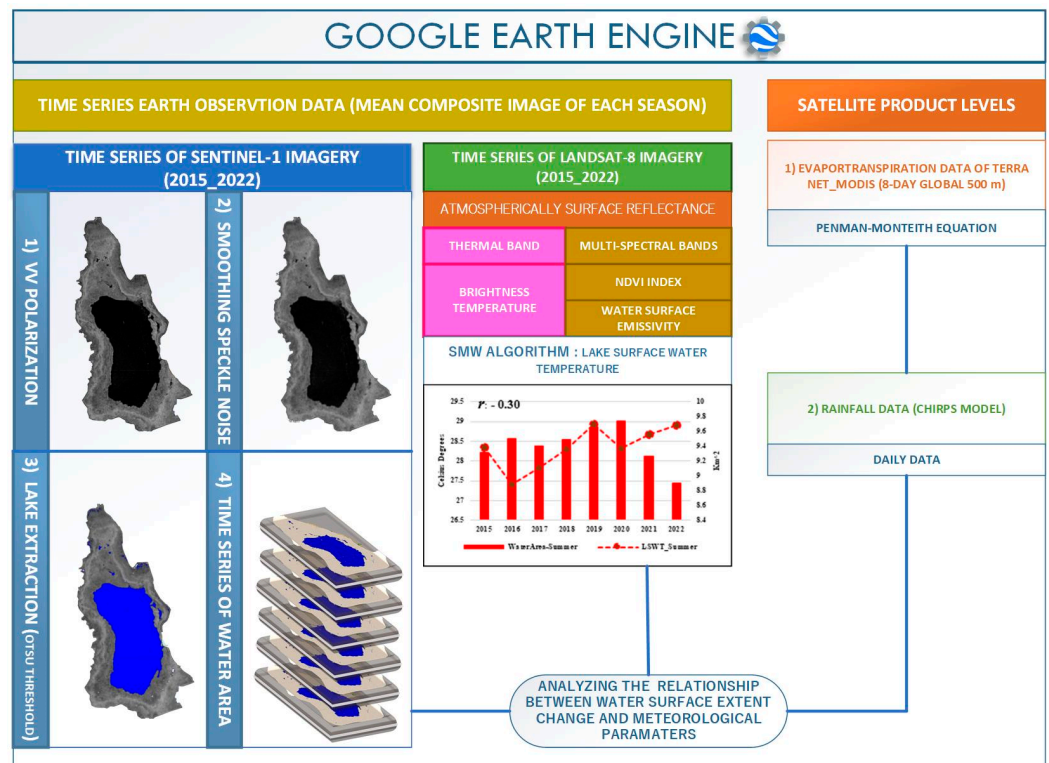
Figure 2. The flowchart of the applied methodology for LWB.

3.1. Water Surface Extent

To extract the LWB with Sentinel-1 images, VV polarization was used. In the pre-processing step, first, the speckle noise in the images using a Gaussian filter with 5×5 windows were reduced. Then, by applying the Otsu threshold, the water class boundary from the non-water class was separated [23]. Otsu introduces a threshold that maximizes the separation between two classes, where the gray values of the image are divided into two classes: water (C_W) and non-water (C_N). The average values and standard deviation of the water, non-water, and total classes μ_w, σ_w, μ_n, σ_n, μ_T and σ_T, respectively. The probability of occurrence of water class and the probability of occurrence of non-water class are $\omega_W = \Pr(C_W)$ and $\omega_N = \Pr(C_N)$. There is intra-class variance σ_{WC}^2 and inter-class variance σ_B^2, according to Equations (1) and (2):

$$\sigma_{WC}^2 = \omega_W \sigma_W^2 + \omega_N \sigma_N^2 \tag{1}$$

$$\sigma_B^2 = \omega_W (\mu_W - \mu_T)^2 + \omega_N (\mu_N - \mu_T)^2 \tag{2}$$

In the Otsu method, a threshold is selected for the image that separates the two peaks of the histogram of the image. From Otsu's point of view, the optimal threshold limit is the one that maximizes the inter-class variance or minimizes the intra-class variance [24].

3.2. LSWT Variable

In the current research, the module developed by Sofia Merida et al. [25] on the GEE platform was used and accessed on day month year. In this module, it is possible to call the Landsat 4 to 8 series of satellites, and it is possible to automatically estimate the temperature of any condition of the earth's surface, including bare land, green land, water, and snow, according to any condition of emissivity. The method used to estimate the temperature is the statistical mono-window (SMW) method, which was provided by the Climate Monitoring Satellite Application Facility (CM_SAF). Due to its simplicity, this algorithm is easily calibrated and implemented [25]. This module can be implemented for Tier 1 and Tier 2 Landsat TOA and surface reflectance data.

3.3. Meteorological Data Impact on Water Surface Changes

As part of this investigation, following the acquisition of average data for distinct seasons, an analysis was conducted to explore the association between various meteorological parameters and the water surface extent of the lake. This examination involved the utilization of Pearson's correlation coefficient (r^2) as a quantitative measure to assess and quantify the degree of correlation between the meteorological variables and changes in the water surface extent.

4. Result and Discussion

In this research, time series of Sentinel-1 satellite images (VV polarization) and Landsat-8 (NIR, RED, and thermal bands) and also time series of produced products, including CHIRPS data and evapotranspiration data from 8-day MOD16A2 products, have been used. In the time series of Sentinel-1 and Landsat-8 images, the average composite images for each season were used, and the average of each season was obtained in the products of precipitation and evapotranspiration.

4.1. Spatiotemporal Changes of Surface Water Extent

The water area of Zarivar Lake exhibited a non-linear change from 2015 to 2022. Figure 3b, illustrates an upward trend in all seasons between 2015 and 2019, but a decline is evident from 2019 to 2022, resulting in the lowest LWB area in 2022. During spring, the LWB area reached its maximum at 11.25 km^2. Subsequently, it decreased to 10.42, 9.40, and 9.27 km^2 in winter, summer, and autumn, respectively. This pattern suggests that winter and autumn rains contribute to the LWB area's increase, reaching a peak of 11.25 km^2 in spring. However, by summer, it declines to 9.40 km^2 due to water consumption and limited rainfall, further decreasing to 9.27 km^2 by autumn. The autumn rains help to prevent a steep decrease, but they are not able to completely make up for the water lost during the summer.
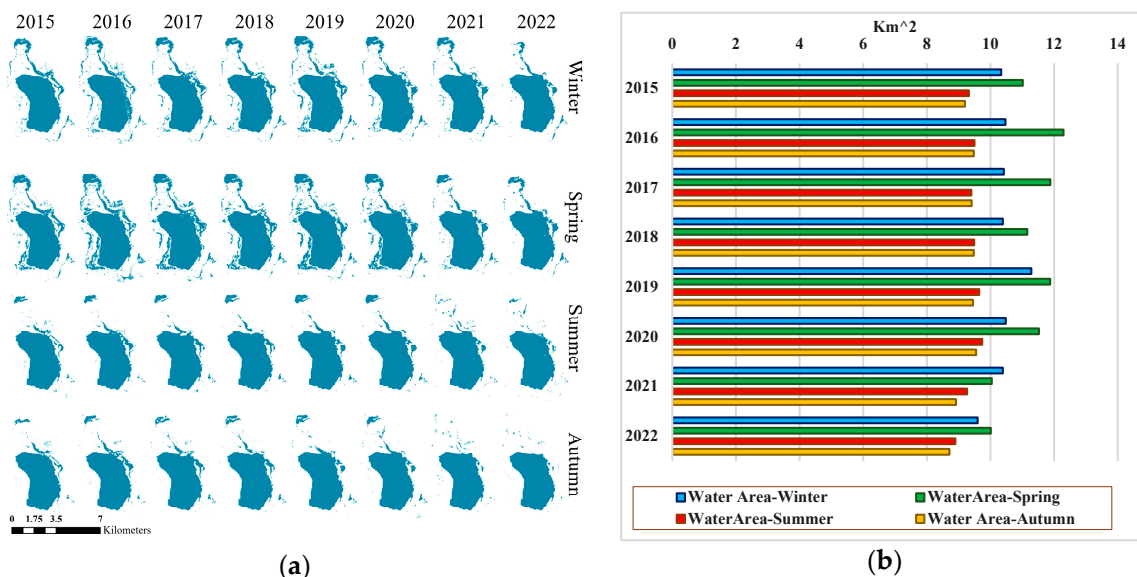

Figure 3. (**a**) LWB map, (**b**) charts of LWB area.

4.2. Rainfall Data and Surface Water Extent Changes

The lake's water supply primarily relies on underground water tables. Seasonal rainfall variations also influence the lake's water area. Strong correlations exist between rainfall and the LWB area, with correlation coefficients of 0.67 and 0.73 in winter and spring, respectively (Figure 4). However, these correlations decrease to 0.30 and 0.31 in summer and autumn. For example, increased winter 2019 rainfall coincided with a peak in the

lake's water area. Subsequently, declining rainfall led to a decreasing water area from 2019 to 2022. Similarly, in spring, higher rainfall in 2015–2016 increased the water area, while lower rainfall in 2018 reduced it. The relationship between precipitation and the water area in summer and autumn follows similar trends, with ups and downs. While autumn rainfall has less impact, a consistent decline in both precipitation and the water area is observed from 2020 to 2022. The correlation coefficients accurately reflect the strong influence of winter and spring precipitation on the lake's water area, while the relationship weakens in summer and autumn due to decreased rainfall compared to the other seasons.
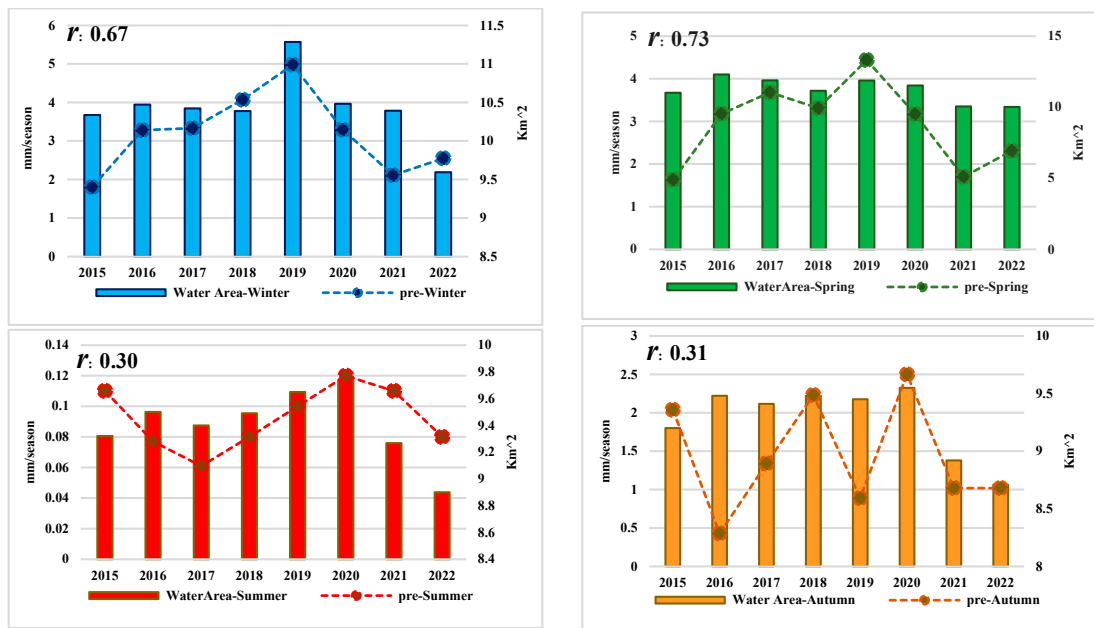

Figure 4. Charts of relationship between LWB area and precipitation.

4.3. LSWT and Surface Water Extent Changes

The relationship between LSWT and the lake's water area yields logical findings. Due to increased water area brought about by lower winter LSWT and higher precipitation, winter exhibits an average LSWT of 4.3 degrees Celsius that correlates weakly ($r = 0.10$). Spring sees an average LSWT of 17.5 degrees Celsius, along with increased spring rains, resulting in a higher correlation coefficient of 0.26. In contrast, during summer, rising LSWT, evapotranspiration, and water consumption for various purposes lead to a decrease in lake water volume and area, yielding a negative correlation coefficient of -0.30. Figure 5 illustrates this inverse relationship in the summer. Autumn, with the onset of autumn rains and high LST and LSWT, shows a correlation of -0.07, moving away from the negative summer relationship and approaching a nearly zero correlation.
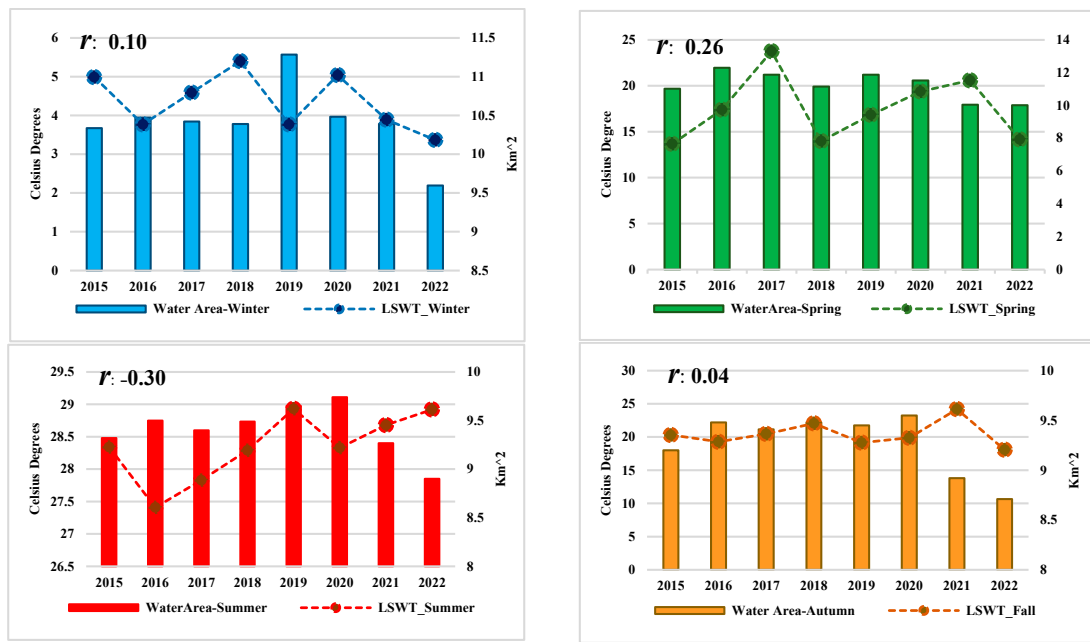
Figure 5. Charts of relationship between LWB area and LSWT.

4.4. Evapotranspiration Data and Surface Water Extent Changes

The positive correlation between evapotranspiration parameters and the waterbody area is consistent across all seasons, with coefficients of 0.49 and 0.46 in winter and autumn, and higher values of 0.59 and 0.60 in spring and summer (Figure 6). On average, evapotranspiration rates are 13.54, 8.45, 7.77, and 5.24 kg/m^2 in spring, summer, winter, and autumn, respectively. This positive relationship is influenced by the wetland nature of Zarivar and its diverse vegetation cover, which contributes to consistent transpiration throughout the year. Furthermore, winter, spring, and autumn precipitation plays a pivotal role in maintaining moisture in the air, soil, and vegetation, thus explaining the positive correlation coefficients in these seasons. In summer, the correlation between water area and evapotranspiration reaches 0.60.
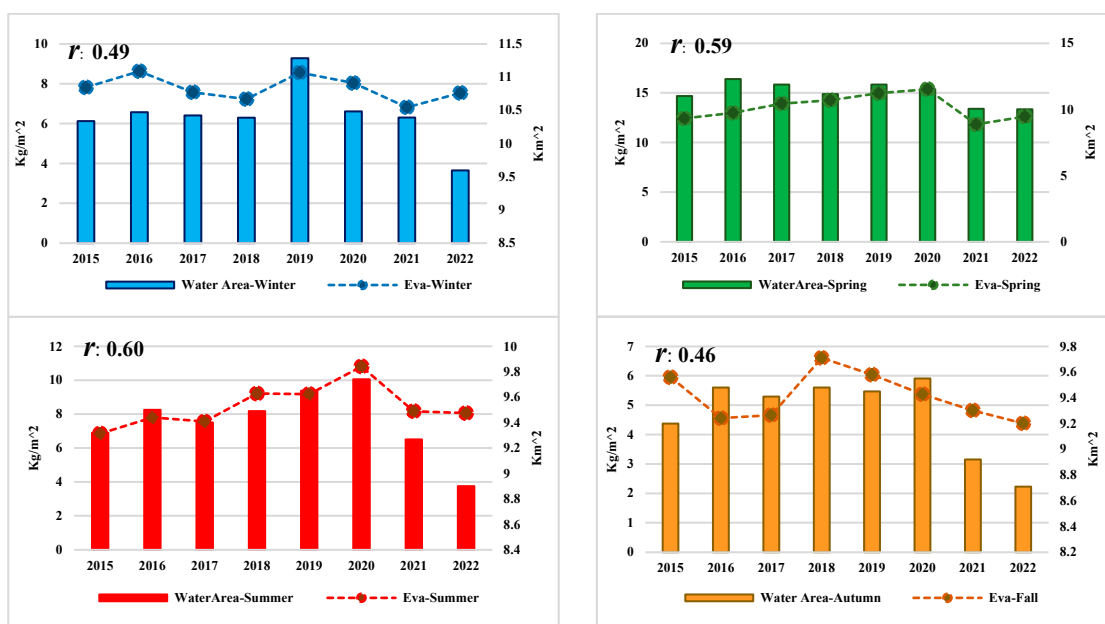

Figure 6. Charts of relationship between LWB area and evapotranspiration.

4.5. Comparative Analysis of Meteorological Data

Investigating the relationship between climate-meteorological parameters helps to better analyze the dynamics of changes in lake water areas. In the previous parts, the relationship between the area of the water zone and the parameters of precipitation, temperature, and evapotranspiration was discussed. The correlation coefficient between precipitation and evapotranspiration is high in spring (0.82), autumn (0.59), winter (0.47), and summer (0.40) based on Table 1. The correlation coefficient between evapotranspiration and LSWT is also shown in Table 1, with values in summer (0.24), autumn (0.20), spring (0.14), and winter (−0.21). These results show that the amount of air humidity in all seasons was higher due to the presence of precipitation. For example, the relationship between LSWT and evapotranspiration in the winter season is opposite, but the relationship between precipitation and evapotranspiration in the same season is equal to 0.47. The correlation coefficient between LSWT and evapotranspiration was higher in summer than in other seasons. This suggests a strong correlation between evapotranspiration and LWB, which can be confirmed by examining the correlation coefficient of precipitation and evapotranspiration.

Table 1. Correlation coefficients between different parameters.

r (Coefficient Correlation)	Winter	Spring	Summer	Autumn
LWB-LSWT	0.10	0.26	−0.30	−0.06
LWB-Precipitation	0.67	0.74	0.30	0.30
LWB-Evapotranspiration	0.49	0.59	0.60	0.46
Precipitation-Evapotranspiration	0.47	0.82	0.40	0.59
LSWT- Evapotranspiration	−0.21	0.14	0.24	0.20

5. Conclusions

This study focused on Zarivar Lake, an important ecological and aquatic ecosystem experiencing water level changes due to climate change and human activities. The research examined the relationship between seasonal variations in the lake's water area and meteorological factors (precipitation, evapotranspiration, and lake surface water temperature) from 2015 to 2022. The results showed clear correlations between the lake's water area and meteorological variables, emphasizing the significant impact of climate change on Zarivar Lake. Conservation efforts are needed to protect this valuable natural resource, and access to data related to underground water is essential for obtaining more accurate results.

References

1. Huang, L.; Xu, X.; Zhai, J.; Sun, C. Local Background Climate Determining the Dynamics of Plateau Lakes in China. *Reg. Environ. Chang.* **2016**, *16*, 2457–2470. [CrossRef]
2. Wu, T.; Hu, X.; Zhang, Y.; Zhang, L.; Tao, P.; Lu, L. Automatic Cloud Detection for High Resolution Satellite Stereo Images and Its Application in Terrain Extraction. *ISPRS J. Photogramm. Remote Sens.* **2016**, *121*, 143–156. [CrossRef]
3. Emami, H.; Zarei, A. Modelling Lake Water's Surface Changes Using Environmental and Remote Sensing Data: A Case Study of Lake Urmia. *Remote Sens. Appl. Soc. Environ.* **2021**, *23*, 100594. [CrossRef]
4. Rickert, B.; van den Berg, H.; Bekure, K.; Girma, S.; de Roda Husman, A.M. Including Aspects of Climate Change into Water Safety Planning: Literature Review of Global Experience and Case Studies from Ethiopian Urban Supplies. *Int. J. Hyg. Environ. Health* **2019**, *222*, 744–755. [CrossRef] [PubMed]
5. Ghanbari, R.; Sobhani, B.; Aghaee, M.; oshnooei nooshabadi, A.; Safarianzengir, V. Monitoring and Evaluation of Effective Climate Parameters on the Cultivation and Zoning of Corn Agricultural Crop in Iran (Case Study: Ardabil Province). *Arab. J. Geosci.* **2021**, *14*, 387. [CrossRef]
6. Jalali, J.; Ahmadi, A.; Abbaspour, K. Runoff Responses to Human Activities and Climate Change in an Arid Watershed of Central Iran. *Hydrol. Sci. J.* **2021**, *66*, 2280–2297. [CrossRef]
7. Ranjbar, S.; Zarei, A.; Hasanlou, M.; Akhoondzadeh, M.; Amini, J.; Amani, M. Machine Learning Inversion Approach for Soil Parameters Estimation over Vegetated Agricultural Areas Using a Combination of Water Cloud Model and Calibrated Integral Equation Model. *J. Appl. Remote Sens.* **2021**, *15*, 018503. [CrossRef]
8. Albarqouni, M.M.Y.; Yagmur, N.; Bektas Balcik, F.; Sekertekin, A. Assessment of Spatio-Temporal Changes in Water Surface Extents and Lake Surface Temperatures Using Google Earth Engine for Lakes Region, Türkiye. *ISPRS Int. J. Geo-Inf.* **2022**, *11*, 407. [CrossRef]
9. Vahid, R.; Farnood Ahmadi, F.; Mohammadi, N. Earthquake damage modeling using cellular automata and fuzzy rule-based models. *Arab. J. Geosci.* **2021**, *14*, 1274. [CrossRef]
10. Yamazaki, D.; Trigg, M.A. The Dynamics of Earth's Surface Water. *Nature* **2016**, *540*, 348–349. [CrossRef] [PubMed]
11. Pekel, J.-F.; Cottam, A.; Gorelick, N.; Belward, A.S. High-Resolution Mapping of Global Surface Water and Its Long-Term Changes. *Nature* **2016**, *540*, 418–422. [CrossRef] [PubMed]
12. Smith, L.C. Satellite Remote Sensing of River Inundation Area, Stage, and Discharge: A Review. *Hydrol. Process.* **1997**, *11*, 1427–1439. [CrossRef]
13. White, L.; Brisco, B.; Dabboor, M.; Schmitt, A.; Pratt, A. A Collection of SAR Methodologies for Monitoring Wetlands. *Remote Sens.* **2015**, *7*, 7615–7645. [CrossRef]
14. Töyrä, J.; Pietroniro, A. Towards Operational Monitoring of a Northern Wetland Using Geomatics-Based Techniques. *Remote Sens. Environ.* **2005**, *97*, 174–191. [CrossRef]
15. Singh, A.; Seitz, F.; Eicker, A.; Güntner, A. Water Budget Analysis within the Surrounding of Prominent Lakes and Reservoirs from Multi-Sensor Earth Observation Data and Hydrological Models: Case Studies of the Aral Sea and Lake Mead. *Remote Sens.* **2016**, *8*, 953. [CrossRef]
16. Lu, L.; Sun, H. Dynamic Monitoring of Surface Water Areas of Nine Plateau Lakes in Yunnan Province Using Long Time-Series Landsat Imagery Based on the Google Earth Engine Platform. *Geocarto Int.* **2023**, *38*, 2253196. [CrossRef]
17. Sadeghi, A.; Galalizadeh, S.; Zehtabian, G.; Khosravi, H. Assessing the Change of Groundwater Quality Compared with Land-Use Change and Precipitation Rate (Zrebar Lake's Basin). *Appl. Water Sci.* **2021**, *11*, 170. [CrossRef]
18. Sulugodu, B.; Deka, P.C. Evaluating the Performance of CHIRPS Satellite Rainfall Data for Streamflow Forecasting. *Water Resour. Manag.* **2019**, *33*, 3913–3927. [CrossRef]
19. Banerjee, A.; Chen, R.; Meadows, E.M.; Singh, R.B.; Mal, S.; Sengupta, D. An Analysis of Long-Term Rainfall Trends and Variability in the Uttarakhand Himalaya Using Google Earth Engine. *Remote Sens.* **2020**, *12*, 709. [CrossRef]
20. Lobell, D.B.; Lesch, S.M.; Corwin, D.L.; Ulmer, M.G.; Anderson, K.A.; Potts, D.J.; Doolittle, J.A.; Matos, M.R.; Baltes, M.J. Regional-scale Assessment of Soil Salinity in the Red River Valley Using Multi-year MODIS EVI and NDVI. *J. Environ. Qual.* **2010**, *39*, 35–41. [CrossRef] [PubMed]
21. Huang, W.; DeVries, B.; Huang, C.; Lang, M.W.; Jones, J.W.; Creed, I.F.; Carroll, M.L. Automated Extraction of Surface Water Extent from Sentinel-1 Data. *Remote Sens.* **2018**, *10*, 797. [CrossRef]
22. Dyba, K.; Ermida, S.; Ptak, M.; Piekarczyk, J.; Sojka, M. Evaluation of Methods for Estimating Lake Surface Water Temperature Using Landsat 8. *Remote Sens.* **2022**, *14*, 3839. [CrossRef]
23. Tran, K.H.; Menenti, M.; Jia, L. Surface Water Mapping and Flood Monitoring in the Mekong Delta Using Sentinel-1 SAR Time Series and Otsu Threshold. *Remote Sens.* **2022**, *14*, 5721. [CrossRef]

24. Xu, X.; Xu, S.; Jin, L.; Song, E. Characteristic Analysis of Otsu Threshold and Its Applications. *Pattern Recognit. Lett.* **2011**, *32*, 956–961. [CrossRef]
25. Ermida, S.L.; Soares, P.; Mantas, V.; Göttsche, F.-M.; Trigo, I.F. Google Earth Engine Open-Source Code for Land Surface Temperature Estimation from the Landsat Series. *Remote Sens.* **2020**, *12*, 1471. [CrossRef]